

Chapter 5

Gait and Anthropometric Profile

Biometrics: A Step Forward

Dimosthenis Ioannidis, Dimitrios Tzovaras, Gabriele Dalle Mura, Marcello Ferro, Gaetano Valenza, Alessandro Tognetti, and Giovanni Pioggia

5.1 Introduction

As of today, biometrics systems are gaining significant attention due to their ability to protect humans and resources from potential non-legitimate user attacks in high security environments (e.g. airports, access control rooms, etc.). It is well known that humans have used body and other characteristics such as face, gait, etc. for recognizing each other (Gloor 1980). The last decades several biometric systems have been developed and established their applicability in controlled environments such as fingerprints, retina and iris, and facial characteristics (Abate et al. 2007; Bowyer et al. 2008; Jain et al. 2004). These technologies have demonstrated reliable user authentication in very restricted environments and the applicability of biometrics to a wider range of surveillance areas stimulated the research community to the

D. Ioannidis (✉) • D. Tzovaras
Informatics and Telematics Institute, 6th km Charilaou-Thermi Road,
P.O. Box 361, Thermi-Thessaloniki 57001, Greece
e-mail: djoannid@iti.gr; dimitrios.tzovaras@iti.gr

G. Dalle Mura • G. Valenza • A. Tognetti
Interdepartmental Research Centre “E. Piaggio”, Faculty of Engineering,
University of Pisa, Via Diotisalvi 2, 56126 Pisa, Italy
e-mail: gabriele.dallemura@iet.unipi.it; gaetano.valenza@iet.unipi.it; a.tognetti@ing.unipi.it

M. Ferro
“Antonio Zampolli” Institute for Computational Linguistics (ILC) National Research
Council (CNR), Via G. Moruzzi 1, 56124 Pisa, Italy
e-mail: marcello.ferro@ilc.cnr.it

G. Pioggia
Institute of Clinical Physiology (IFC), National Research Council (CNR),
Via G. Moruzzi 1, 56124 Pisa, Italy
e-mail: giovanni.pioggia@ifc.cnr.it

design and development of new and emerging biometrics such as gait (Boulgouris and Chi 2007) and characteristics based on user anthropometric profile (e.g. full or partially body measurements) (Ferro et al. 2009). Current work on these approaches demonstrated their authentication potential and their ability to allow the non-stop authentication of the humans in high security environments. However, since these biometric techniques (activity-related signals and body measurements) are mature, more experimental frameworks shall be designed and evaluated for human verification in order to fully deploy them in large-scale security applications. In the following sections, two unimodal biometric traits are presented based on the analysis of body measurements either using dynamic signals (gait) or analyzing body in fixed seat environment (body measurements using a sensing seat sensor).

5.2 On the Potential of Body Measurements for User Authentication

5.2.1 Authentication Potential of Gait as a Biometric

The last 10 years, gait as a biometric has received significant attention due to increase in the importance of surveillance and security in public and private areas. Latest research activities in multi-biometric environments have evolved the use of gait as a promising modality for identification and authentication purposes. The current state of the art is that “databases of over 100 subjects imaged walking outdoors or indoors can be recognised with well over 90% identification rate and factors which affect gait were understood, there was capability to handle application environment and understanding of the measure’s potency for recognition purposes” (Gloor 1980). However, recognition rates with change of view angle, clothing, shoe, surface, illumination, and pose usually decreased performance, thus making the human gait recognition a challenging and emerging biometric trait (Boulgouris et al. 2005).

Recent studies on the gait recognition potential are focused mainly in two directions: view-invariant gait analysis (Jean et al. 2009; Bodor et al. 2009; Bouchrika et al. 2009) and novel algorithms for the extraction and fusion of static and kinematic parameters of human locomotion (Chen et al. 2009; Bouchrika and Nixon 2008). In most cases, gait recognition is comprised from two main phases: a feature extraction phase, where motion information is obtained and recognition phase, where a classification technique is applied to the obtain motion patterns. The crux of the gait recognition lies in perfecting the first phase. It is challenging to specify gait features that are sufficiently discriminable and can be reliably extracted from video. The methods utilised for this feature extraction can be broadly classified as being either model-free (appearance-based) or model-based. Appearance-based methods focus on the spatiotemporal information contained in the silhouette images. Model-based methods construct human model to obtain explicit features describing gait dynamics, such as stride dimensions and joint kinematics.

A recent study using model-based approach (five-link biped model) reported recognition rates of 100% in the CMU MoBo data set (25 subjects) (Zhang et al. 2007). When examining a greater data set, Bouchrika and Nixon (2007) reached a correct classification rate of 92%, again, by means of model-based approach. In their study the motion templates describing the motion of the joints as derived by gait analysis, were parameterised using the elliptic Fourier descriptors. The mean error for the extracted joints compared to manual data (10 persons) was 1.36% of height. However, in both model-based approaches the camera was capturing the side-view of the subjects. Promising results for a frontal-view gait recognition have been demonstrated by Goffredo et al. (2008) by means of an appearance-based approach. The proposed method for the front-view gait analysis is based on two consecutive steps: the gait cycle detection and the gait volume description. Without any knowledge of the camera parameters the authors found a mean percentage of recognition rate equal to 96.3%, when examining three public available databases.

Concluding, both model- and appearance-based approaches have increased their performance in gait recognition the last years. When examining gait recognition under several certain view angles (especial frontal or near frontal view) appearance-based approaches seem to outperform the model based approaches. However when the issue is an approach, which should be independent from viewpoint, i.e. enrolment and test are taking place at different view angles, model based methods seem to be more appropriate. It is possible that a fusion of model- and appearance-based approaches can contribute to higher rates, whereas the static and dynamic cues of gait are extracted using compact representations with robust performance in dynamic changing environments.

5.2.2 Authentication Potential of Body Measurements as a Biometric

Several companies are currently working to realize comfortable interactive seats. These systems, some of them already on the market, use different technologies and materials, but they share the use of sensors that measure the pressure exerted on the seat by the subject. Actually, the existing sensing seats are not able to perform the human authentication task and no result on this topic, even if in a preliminary stage, was found in literature review. The BPMS by [Tekscan](#) measures the pressure distribution of a human body on support surfaces such as seats, mattresses, cushions, and backrests and it is used for automotive driver seat design, hospital and home seat design, comfort analysis. The study developed by Tan et al. (2001) is focused on sensing chair using pressure sensors placed over the seat pan and back rest of the chair for real-time capturing of contact information between the chair and its occupant in order to implement static posture classification. A kind of technology, developed in the textile domain, is Softswitch (The Softswitch Company 2008: it is based on pressure sensors that can be integrated in fabrics. Softswitch combines conductive

textile materials and a quantum tunnelling composite (QTC) with unique pressure controllable switching properties. The research of seating comfort in the transportation industry is still an open problem; for solving this question some studies (The Johnson Controls Company 2008) have been effected to evaluate the advantages and the disadvantages of automotive seat. It is possible to note that the presented systems are more focused on comfort monitoring, pressure mapping, air-bag activation and event-related tasks. However, the information supplied by these systems may be used to extract features useful for the authentication task, as for instance pressure profile. UNIPI, starting from this consideration, works to realize a system for subject authentication based on sensing seat. The first prototype of this system is part of the HUMABIO (Human Monitoring and Authentication Using Biodynamic Indicators and Behavioral Analysis) project for multi-modal human authentication. HUMABIO is a EC co-funded Specific Targeted Research Project (STREP) where new types of biometrics were combined with state of the art sensor technologies in order to enhance security in a wide spectrum of applications like transportation safety and continuous authentication in safety critical environments like laboratories, airports or other buildings. In this project, the enrolment and the authentication procedures were carried out with the cooperation of the user, according to the instructions supplied by the system. The mentioned prototype is able to supply a one-dimensional deformation profile, and, after a feature extraction process, the system is able to perform the human authentication task. The ACTIBIO project aims to perform a continuous authentication, without interfering with the user actions and according to the detection of predefined events. According to this purpose, the previous SensingSeat prototype was upgraded and a new control system was developed to handle the issues regarding the continuous authentication as well as the event notifications of the ACTIBIO core system.

5.3 Gait Biometric Technology

5.3.1 *Proposed Approach and Motivation*

The main purpose and contributions of this paper are summarized as follows:

- A novel gait recognition system is proposed based on the use of 2D and new 3D appearance-based features of the image silhouette sequence.
- Three novel feature extraction techniques are presented: the two of them are based on the generalized Radon Transform, namely the Radial Integration Transform (RIT) and the Circular Integration Transform (CIT), whilst the third descriptor is based on the weighted Krawtchouk moments. The former are utilized in order to provide an analytical representation of the static and dynamic cues of the human body shape using a few coefficients, and the latter, are well known for their discriminating capability and compactness.

- The paper also introduces the use of range data, captured by a stereo camera, for gait signal analysis. Depth related data are assigned to the binary image silhouette sequences using an innovative transform: the 3D Geodesic Silhouette Distribution Transform. This transform is utilized to encode information about the position of the human body segments on the image plain and their 3D distribution on the hull that depicts the visible human body.

The proposed algorithms were tested and evaluated in two main different databases, namely the “Gait Challenge” of USF and in the proprietary gait database of the HUMABIO EU IST project consisting of 75 persons. Extensive experiments have been carried out in these databases and the proposed methods were found to be robust in existence of noise and with increased recognition accuracy, when compared to other similar state-of-the-art algorithms.

5.3.2 Silhouette Extraction and Pre-processing Steps

5.3.2.1 Background Estimation and Binary Silhouette Extraction

The first step in a human gait recognition system that uses appearance-based techniques is the extraction of the walking subject’s silhouette from the input color image sequence. In this paper, a sequential number of steps are introduced in order to provide the final binary silhouettes, as illustrated in Fig. 5.1.

Initially, the background is estimated using a temporal median filter on the image sequence, assuming that the background is static and the foreground is moving. In the next step, the silhouettes, denoted as B_k^{Sil} , are extracted by comparing each frame of the sequence with the background. The areas where the difference of their intensity from the background image is larger than a predefined threshold are considered as silhouette areas. The silhouette images that are extracted by this method are noisy. Therefore morphological filtering, based on anti-extensive connected operators (Salembier and Marqués 1999) is applied in order to denoise the binary silhouettes. Finally, potential shadows are removed by analyzing the sequence in the HSV color space (Cucchiara et al. 2001), as illustrated in Fig. 5.1d.

5.3.2.2 Silhouette Enhancement Using Range Data

A novel technique is introduced that exploits range data, if they are available. At this stage, each gait sequence is composed of k preprocessed binary silhouettes \tilde{B}_k^{Sil} . Initially, the triangulated version of the 3D silhouette that also includes depth information is generated. Then, using Delaunay triangulation on the available range data, the 3D hull (Moustakas et al. 2007), for each image of the gait sequence is estimated and finally using the Geodesic Transform (Ioannidis et al. 2007) the 3D Geodesic silhouette is extracted, denoted as $\hat{G}_k^{Sil}(x, y)$. Figure 5.2 depicts extracted (a) binary silhouettes and (b) their corresponding 3D geodesic distributed silhouettes.

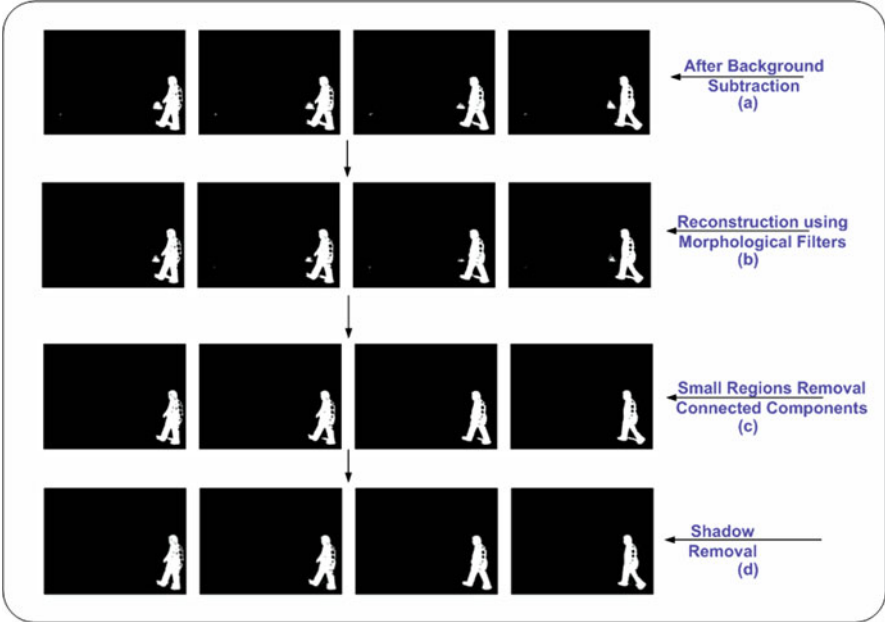


Fig. 5.1 Denoising the initial silhouette images (a) using morphological filters (b), connected component labelling (c) and shadow suppression in terms of HSV colour space (d)

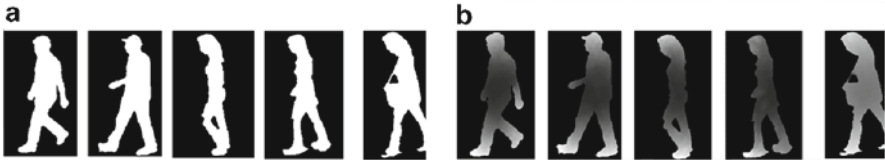


Fig. 5.2 Illustration of silhouette representation used by the proposed system, (a) binary silhouette, (b) 3D geodesic distributed silhouette

In the final step of the preprocessing stage, the denoised binary (\tilde{B}^{Sil}) or 3D silhouette sequence (\hat{G}^{Sil}) are scaled and aligned to the center of the frame in each frame (Sarkar et al. 2005).

5.3.3 Feature Extraction Phase

In this paper, three appearance-based techniques are employed in order to extract the most discriminative characteristics of the human locomotion. In all cases, the input to this phase of the gait system is assumed to be either the binary silhouettes (\tilde{B}_k^{Sil}) or the 3D-Geodesic image sequence (\hat{G}_k^{Sil}).

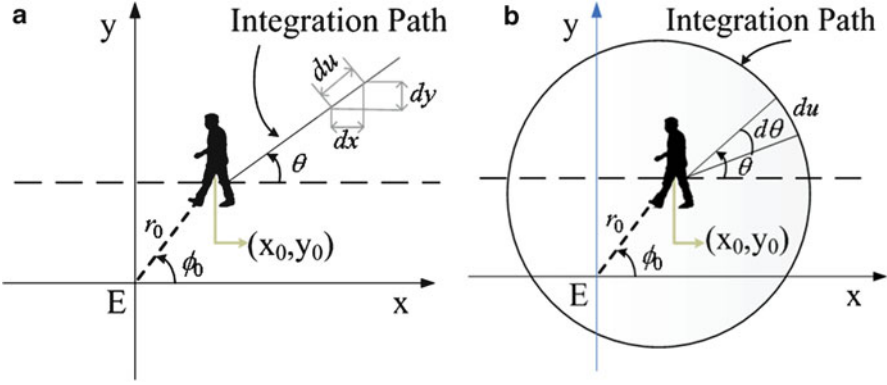


Fig. 5.3 Applying the RIT (a) and CIT (b) transforms on a silhouette image

5.3.3.1 Generalized Radon Transformations

Two one-dimensional Radon transformations are introduced for feature extraction, namely the Radial Integration Transform (RIT) and the Circular Integration Transform (CIT), which are proven to provide a full analytical representation of the human silhouette (Daras et al. 2006). In particular, the RIT of a function $f(x,y)$ is defined as the integral of $f(x,y)$ in the direction of a straight line starting from the point (x_0, y_0) and forming angle θ with the horizontal axis x (Fig. 5.3). In the proposed approach, the discrete form (Daras et al. 2006) of the RIT transform is used:

$$RIT(t\Delta\theta) = \frac{1}{J} \sum_{j=1}^J Sil(x_0 + j\Delta u \cdot \cos(t\Delta\theta), y_0 + j\Delta u \cdot \sin(t\Delta\theta)) \quad (5.1)$$

where $t = 1, \dots, T$, Δu and $\Delta\theta$ are the constant step sizes of the distance (u) and angle (θ), J is the number of silhouette pixels that coincides with the line that has orientation θ and are positioned between the center of the silhouette and the end of the silhouette in that direction, Sil represents the correspondent binary or 3D silhouette image, and finally $T = 360^\circ / \Delta\theta$.

In a similar manner, CIT is defined as the integral of a function $f(x,y)$ along a circle curve $h(\rho)$ with center (x_0, y_0) and radius ρ and its discrete form that is utilized by the proposed gait system is given by:

$$CIT(k\Delta\rho) = \frac{1}{T} \sum_{t=1}^T Sil(x_0 + k\Delta\rho \cdot \cos(t\Delta\theta), y_0 + k\Delta\rho \cdot \sin(t\Delta\theta)) \quad (5.2)$$

where $k = 1, \dots, K$, $\Delta\rho$ and $\Delta\theta$ are the constant step sizes of the radius and angle variables, $K \Delta\rho$ is the radius of the smallest circle that encloses the binary or 3D silhouette image Sil , and finally $T = 360^\circ / \Delta\theta$.

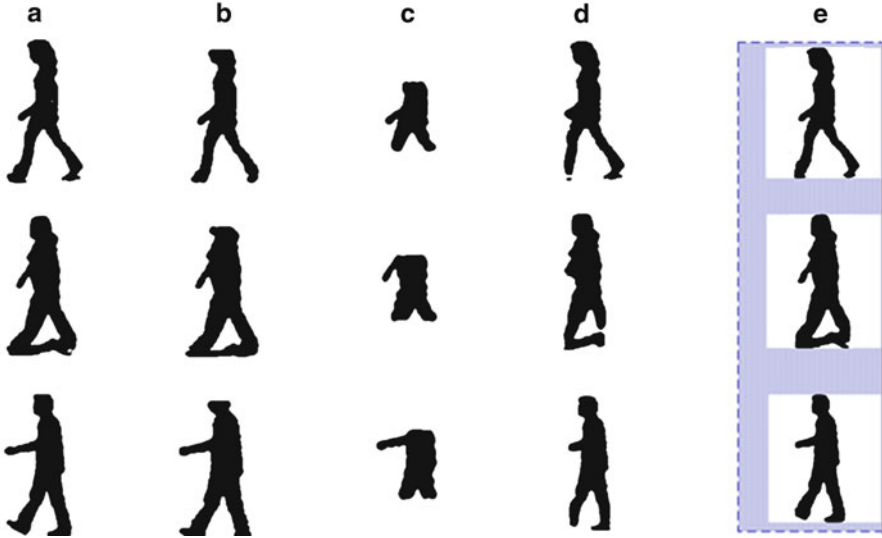


Fig. 5.4 Reconstruction of silhouette images using Krawtchouk moments for different moment order values (N, M), (a) Original Silhouette ($W \times H = 188 \times 200$), (b) $N = W/10, M = H/4$, (c) $N = W/10, M = H/16$, (d) $N = W/30, M = H/2$ and (e) $N = W/15, M = H/3$

5.3.3.2 Orthogonal Discrete Transform Using Krawtchouk Moments

In this work, a new set of orthogonal moments is proposed based on the discrete classical weighted Krawtchouk polynomials (Mademlis et al. 2006). These moments are proposed due their capability to extract local shape characteristics of images and in addition their orthogonality ensures minimal information redundancy. The Krawtchouk moments Q_{nm} of order $(n+m)$ are estimated using the weighted Krawtchouk polynomials for a silhouette image (binary or 3D) with intensity function $Sil(x, y)$ as follows:

$$Q_{nm} = \sum_{x=0}^{N-1} \sum_{y=0}^{M-1} \bar{K}_n(x; p, N-1) * \bar{K}_m(y; p, M-1) \cdot Sil(x, y) \quad (5.3)$$

$$\bar{K}_n(x; p, N) = K_n(x; p, N) \sqrt{\frac{w(x; p, N)}{\rho(n; p, N)}} \quad (5.4)$$

where \bar{K}_n, \bar{K}_m are the weighted Krawtchouk polynomials, and $(N-1) \times (M-1)$ represents the pixel size of the silhouette image. Figure 5.4 shows a graphical representation of the reconstructed silhouette images using different orders of N (for width) and M (for height).

Table 5.1 Comparative verification rates P_v of the proposed optimal weighted features (RCK-G) and the baseline algorithm (Sarkar et al. 2005) at a false rejection rate of 1%, and 10% using z-Norm scores and the binary silhouette transform, due to the lack of range data in the USF database

	ZN (z-Norm)		ZN	
	P_v (%) at P_{FRR} 1%		P_v (%) at P_{FRR} 10%	
	RCK-G	USF	RCK-G	USF
A	92	86	99	96
B	88	76	97	90
C	72	59	93	80
D	46	42	78	70
E	41	52	78	60
F	25	41	64	60
G	32	36	67	45

5.3.4 Signature Matching

The following notations are used in this section: the term gallery is used to refer to the set of reference sequences, whereas the test or unknown sequences to be verified or identified are termed probe sequence. An important step in the recognition system, formally before the matching stage, is gait cycle detection of the gallery/probe sequence. In this paper, the gait cycle is detected using a similar approach to Boulgouris et al. (2004), whereas the signature matching is based on the method described analytically in Ioannidis et al. (2007). Specifically, for each classifier of the proposed system, a distance score is estimated between the probe and the gallery $D_r(\text{Probe}, \text{Gallery})$. Finally, the final distance is calculated based on the weighted algorithm (RCK-G) that is presented analytically in Ioannidis et al. (2007).

5.3.5 Experimental Results and Conclusions

The proposed methods were evaluated on two different databases: (a) the publicly available HumanID “Gait Challenge” dataset (Sarkar et al. 2005), and (b) the proprietary large indoor HUMABIO dataset (Ioannidis et al. 2007). For evaluation of the proposed approach in a verification scenario, Rate Operating Characteristic curves (ROC) are used that illustrate the probability P_v of positively recognizing an authorized person for different values of the false acceptance rate P_{FAR} .

Verification results on USF dataset for RCK-G algorithm are reported in Table 5.1 in comparison with the baseline algorithm (Sarkar et al. 2005).

As seen, the proposed method based on the silhouette sequences and using the weighted classifiers generally outperforms the baseline method. Using the normalized distances-scores, the verification performance is improved, e.g. for a false rejection rate of 10% the verification rate is above 64% for all experiments A-G.

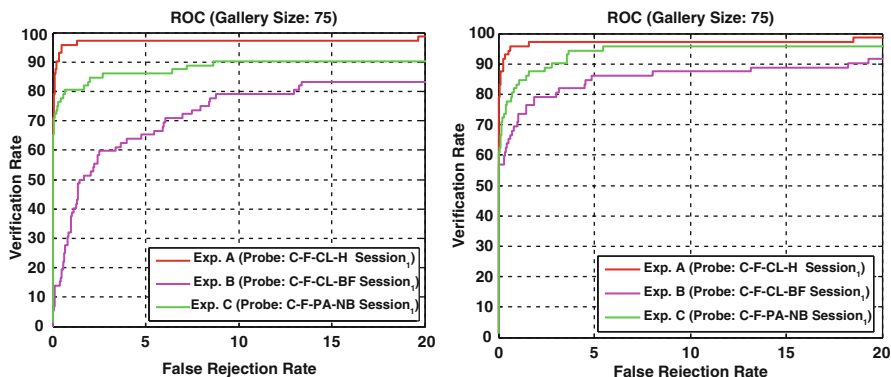


Fig. 5.5 Rate Operating Characteristic (ROC) curves for the HUMABIO gait database using the weighted classifiers (RCK-G) and normalized scores (zNorm) based on the Binary Silhouette Transform (*left*) and the Geodesic Silhouette Distribution Transform (*right*)

Verification results are also reported for the HUMABIO gait database. The ROC using the z-Norm scores of the weighted feature algorithm (RCK-G) is shown in Fig. 5.5. Verification rates are increased when 3D silhouette sequences were used instead of the binary silhouettes. For example, for a false rejection rate of 5% the verification rate is increased by 6% for shoe (experiment C) condition, when Geodesic silhouette distribution transform is used.

In this section, a novel feature-based gait recognition framework was presented that uses the 2.5D information of the captured sequence captured by a stereo camera. This information is initially transformed into a 3D hull and then the 3D protrusion transform is proposed to generate the “geodesic” silhouette. Three novel feature extractor algorithms are combined together using a weighted algorithm in order to extract the static and dynamic cues of the human gait shape either in the binary silhouette or in the geodesic silhouette distribution. Experimental results demonstrate the efficiency of the proposed method when compared to state of the art approaches.

5.4 An Innovative Sensing Seat for Human Authentication

5.4.1 Sensing Seat Technology

The UNIPI module is an unobtrusive and versatile sensing seat system for human authentication that can be employed in different scenarios such as truck and car pilots, airplane pilots, plant and office personnel, and, in general, environments where the security is mandatory and a soft seat is available. It is an anthropometric system based on pressure sensors integrated in seats, in order to enhance the security and reliability of the other biometric system but also increase its applicability to scenarios where the physiological profile of an individual cannot be obtained.

The sensing seat is realized by a seat coated by a removable Lycra sensing cover. The sensing cover is able to respond to simultaneous deformations in different directions by means of a piezoresistive network which consists of a mixture of polymers deepened with coal directly printed onto the fabric. The strain sensors developed by the University of Pisa are realized by means of Conductive Elastomers (CE) composites (Lorussi et al. 2004, 2005). CE composites show piezoresistive properties when a deformation is applied and can be easily integrated into fabric or other flexible substrate to be employed as strain sensors. The used CE is based on a WACKER Ltd (Elastosil LR 3162 A/B) product (The Wacker Company 2008). It consists in a mixture of graphite and silicon rubber. WACKER Ltd guarantees the non-toxicity of the product that, after the vulcanization, can be employed in medical and pharmaceutical applications. It can be smeared on flexible and elastic substrate or arranged in films applicable on elastic supports. Sensors were realized by directly smearing the CE on a Lycra®-cotton fabric previously covered by an adhesive mask. The mask is designed according to the shape and the dimension desired for the sensors. The production phase is structured as follows: after depositing the material, the mask is removed and the treated fabric is placed in an oven at about 130°C. During this phase the cross-linking of the solution speeds up and, in about 10 min, the sensing fabric is ready to be employed. It is important to underline that the integration of CE materials does not change the mechanical properties of the underlying texture, thus maintaining a good comfort for the user. For a correct determination of sensor positions and orientations, experimental trials were performed in order to validate the proposed design. To obtain a specific sensor topology over the fabric, an adhesive mask representing the drawing of sensors and connections was realized. The mask is designed starting from the desired sensor positions and orientations traced on a three-dimensional model of the human body. Then, the mask is realized by cutting a sheet of adhesive paper with a laser milling machine.

5.4.1.1 Static and Dynamic Characterization of Conductive Elastomeric Sensor

The piezoresistive properties of CE composites, in literature, are statically described by using percolation theory. In our work, the attention has been focused on the behavior of the electrical resistance of CE during the transient time and other non-linear phenomena occurring after a deformation. In our application, CE has been integrated into fabric and employed as strain sensors. The main objective of the CE characterization has been to determine the relationship between the electric resistance $R(t)$ of a CE sample and its actual length $L(t)$, where t is the time.

For instance, in terms of quasi-static characterization (Lorussi et al. 2005), a CE sample of 5 cm in length and 1.7 cm in width presents an non-stretched electrical resistance of about 3KOhm per cm, and its gauge factor (GF) is about 2.9. In order to obtain the gauge factor, it is necessary to construct the static calibration curve shown in Fig. 5.6.

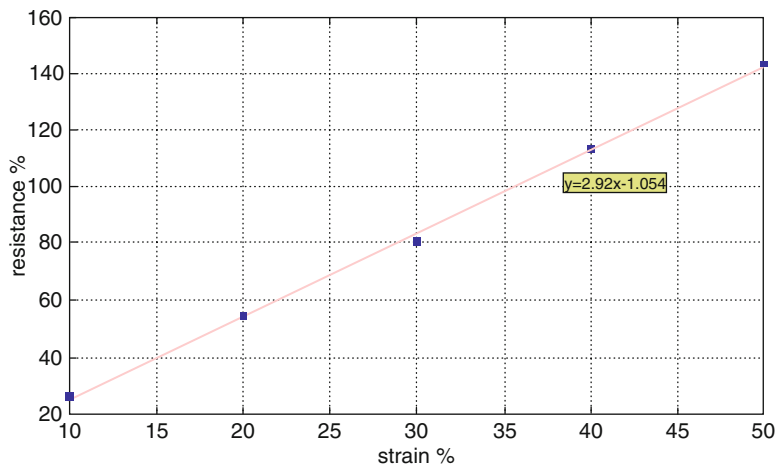


Fig. 5.6 The static calibration curve

The curve is realized by stretching the CE sample with the step in deformation having different strain (Fig. 5.7) and at the same time acquiring the final resistance value (Scilingo et al. 2003). The GF represents the angular coefficient of the static calibration curve.

Sensor response shows a peak in correspondence to every mechanical transition. Sensor responses during constant pressure time intervals may be approximated by decreasing exponential, assuming the local minimum as the steady-state value. The longer the pressure time interval, the more the above mentioned approximation is accurate. In order to remove the contribution of high order exponential, the first order time constants were extracted by means of a window filter. This choice allowed quantization errors introduced by the acquisition device in response to rapid transitions to be avoided and sensor steady state deformation, related to slower frequency components, to be maintained. Taking into account the first-order components of the sensor response (resistance variation) to a rectangular stimulation (applied deformation), the equivalent circuit represented in Fig. 5.8 can be derived.

The power supply V is the electrical equivalent of the imposed deformation. The switch T1 (initially open) is closed and opened in correspondence to the beginning and the end of the imposed deformation respectively. The switch T2 (initially open) is closed when T1 is opened again. Following a simple analysis of this circuit, it is easy to recognize that the variation of the charging and discharging currents of the capacitance in consecutive phases of stimulation are equivalent to the variation of the resistance of the sensor during its deformation and the following release respectively. The circuit parameters R_1 , R_2 , R_3 and C can be derived by using the features, extracted from reference experimental signals, listed in Table 5.1. The features values listed above were extracted from ten cycles of a reference experimental signal and were used to derive the circuit parameters.

According to these ten cycles of stimulation, the solution of this equivalent circuit provided the results reported in Fig. 5.9.

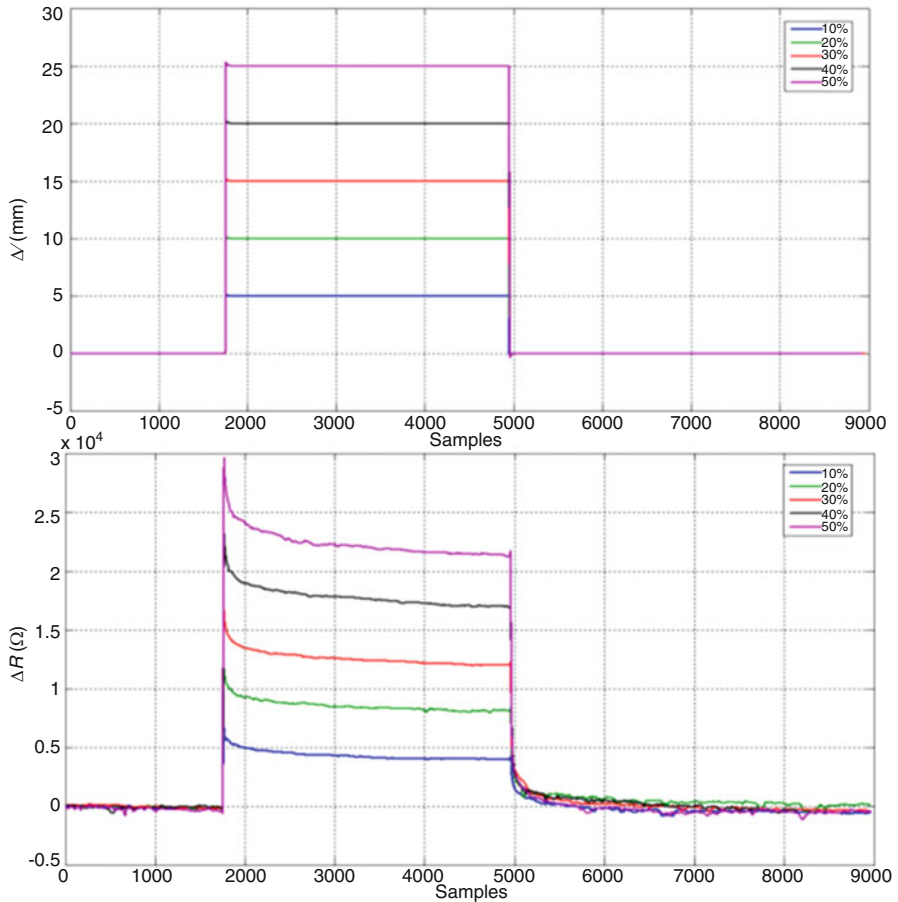


Fig. 5.7 Response of a CE sensor excited by step in deformation to build the static calibration curve

Figure 5.10, which has been reported as an example of this analysis, shows the output of a sample stretched with trapezoidal ramps in deformation having different velocities $\dot{L}(t)$ (where $L(t)$ is the length of the sample).

The main remarks on sensor behavior are summarized in the following:

- Both in the case of deformations which increase or decrease very quickly the length of the specimen and in the case of deformations which reduce it, two local maxima greater than both the starting and the regime value are shown.
- If the relationship between $R(t)$ and $L(t)$ were linear, one of the extreme described in the previous point would be a minimum.
- The height of the overshoot peaks increases with the strength velocity $\dot{L}(t)$.
- The relaxing transient time, which lasts up to several minutes, is too long to suitably code the human movements.

Fig. 5.8 Electric model of a conductive elastomeric strain sensor

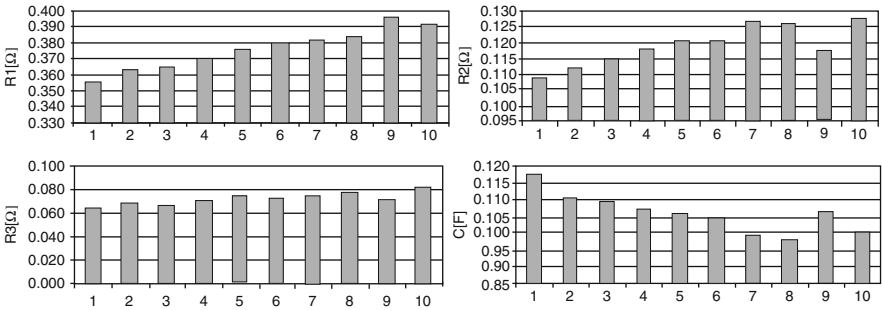
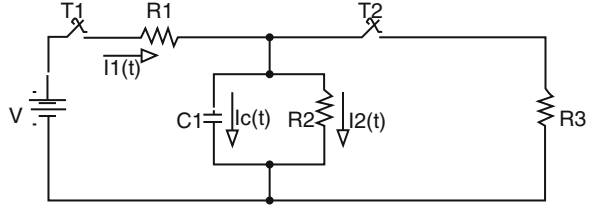


Fig. 5.9 Values of the parameters of the equivalent electric model extracted from ten cycles of a reference experimental signal

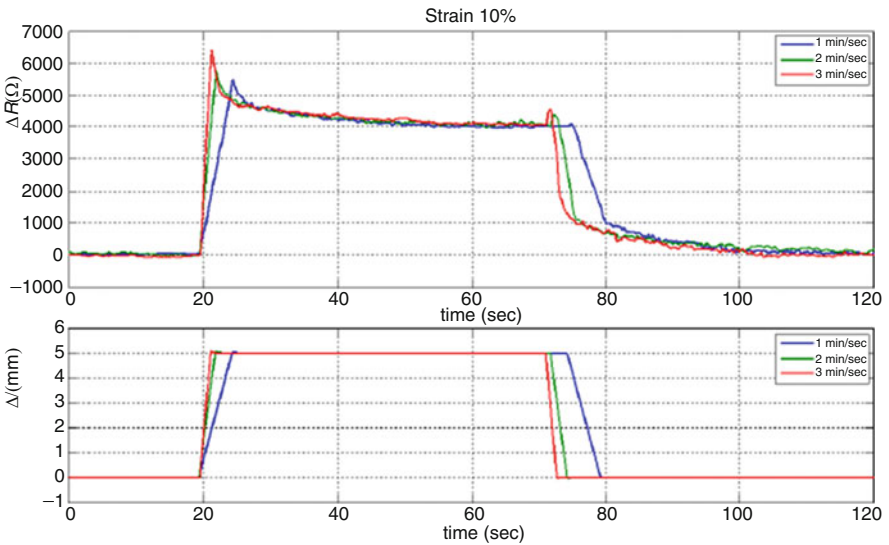


Fig. 5.10 Response of a CE sensor excited by trapezoidal ramps in deformation

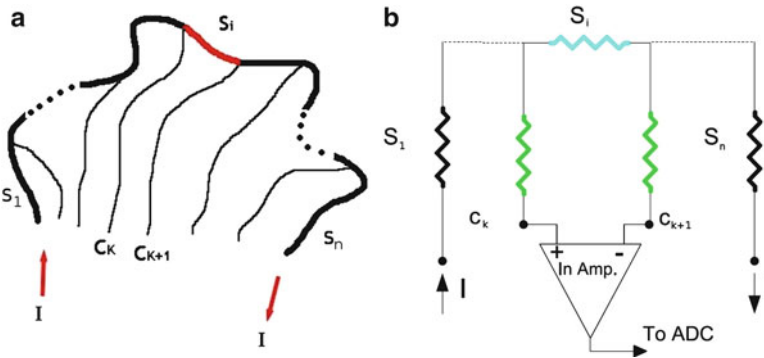


Fig. 5.11 Sensing cover electrical model (a) and electronic acquisition front-end (b)

5.4.1.2 Electrical Model and Acquisition Electronic Design

The sensors and their connections to the acquisition unit was realized by means of the same materials, in this way no metallic cables are needed on the seat. This is an advantage in terms of user comfort as we maintain the fabric original elasticity. Moreover, by using this approach, the electrical contacts on the CE material can be placed in areas where the fabric deformations and stresses are reduced. Figure 5.11a, b represent the generic configuration of a sensing cover and the electronics acquisition front-end respectively. The sensors are connected in series thus forming a single sensor line (larger line of Fig. 5.11a) while the connections (represented by the thin lines of Fig. 5.11b) intersect the sensor line in the appropriate points.

Since connections and sensors are made by the same material, both of them change their electrical resistance when the user moves. For this reason, the front-end of the acquisition unit had to be designed in order to compensate the connection resistance variations. To obtain this result, the sensor line is supplied with a constant current I and the voltage falling across two consecutive connections are acquired using high input impedance amplifiers (i.e., instrumentation amplifiers), as shown in Fig. 5.11b. Considering the example of sensor S_i , if the amplifier is connected between C_k and C_{k+1} , only a little amount of current flows through the connection lines compared to the current that flows through the sensor line (and in the sensor S_i). In this way, if the current I is well dimensioned, the voltage read by the amplifier is almost equal to the voltage fall across the sensor (that is proportional to the sensor S_i electrical resistance). Taking into account the above described strategy, the analog front-end of the electronic unit included a number of instrumentation amplifiers equal to the sensors number. The data coming from the front-end, are low pass filtered, digitalized and acquired in a PC by means of a general purpose card or transmitted by a dedicated electronic interface. Moreover, the power consumption is near zero resulting in a completely safe system. The fabric equipped with distributed and redundant unobtrusive strain sensors guarantees to address plasticity, low dimension, lightness, and low cost. Since the strain sensors can be directly printed on the

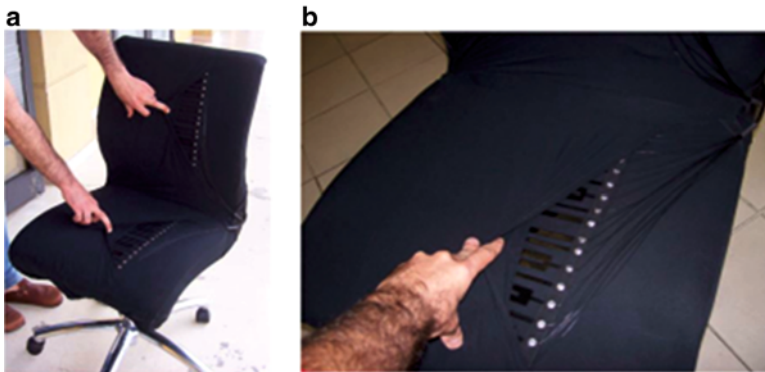


Fig. 5.12 The Sensing Seat system prototype: (a) The office seat equipped with the sensing cover; (b) details of the sensor connections on the bottom side of the sensing cover

fabric, specific cover layouts may be designed to coat different seat shapes obtaining a good adherence to the seat. As a result, the sensing seat system does not interfere with the mechanical structure of the seat and it is designed as an extension of the seat itself (Fig. 5.12).

5.4.2 Sensing Seat Experimental Results

5.4.2.1 Recording Protocol and Data Analysis

Several topology layouts were taken into account (series, parallel and quadrupole network of sensors) and finally the best compromise between the technical complexity and the classification performance of the system was found using the series network. The sensing cover prototype is equipped with 32 strain sensors: 16 sensors in the bottom side and 16 in the upper side. The existing sensing cover prototype was tailored to a real office seat. Different layouts could be developed to handle different types of seats (e.g. office seats, car seats). It should also be remarked that the seat must be soft enough to guarantee the sensors to be adequately stretched as a human subject is seated. Moreover, as it will be explained below, since the signals supplied by the sensors depend on the positioning and the initial stretching of the cover, data are consistent only after the cover is mounted over the specific seat. In fact, the enrolment signatures are not valid if the cover is dismounted and mounted again even on the same seat. In a normal scenario, once the sensing cover has been mounted, it should not be removed. However, in order to overcome this inconvenience, UNIPI studied some solutions. The best way is a kind of automatic recalibration. When the sensing cover is removed and mounted again, unavoidably the initial deformation of the cover is different, and consequently the electrical signals too. The recalibration phase needs only two steps: the signals in no-seated and in

full-seated condition. With these information, using an interpolation function, it is possible to map the status of the sensors from the previous configuration into the current one. In this way, only using a scale factor, it is possible to adapt the previous signature and no new enrolment phase is necessary. Some methods to extract the features were tested, and the one, among the others, having the best performance in term of classification, was the method using as features the minimum, maximum and mean values, and this one was implemented. In this way during an action the 32 signals from the sensorized cover are acquired and stored, and the start and stop action time are taken in account. The initial and final 5% of the entire time period are not considered for the analysis in order to bypass the transitory signal phenomena. The remaining part of signal is elaborated in order to extract the minimum value, the maximum value and the mean value. This process is done over all the 32 signals. At this point, this matrix of values recorded during the enrolment phase forms the biometric signature of a particular subject performing a particular action, and all the signatures are stored into a database. This process is done over all the subjects and over all the actions. During the authentication phase, the features are extracted with the same strategy and then they are compared with the stored signature using a classifier. Some classifiers were tested in order to evaluate the recognition phase. On the base of the results, the classifier based on the Euclidean vector distance was chosen. No specific protocol is required to extract the features, since the recording protocol is very adaptable. Only the subject is asked to start from full-seated position and to return in the same position after to have performed the action. Since these elements are linked to the deformation of the sensors due to the subject pressure, each signature represents the deformation of the seat. As a result, the voltage vectors available for each measurement and for each predefined position are related to the pressure exerted by the subject on the seat (Ford Global Technologies Inc. 2001; Hilliard 2002; Federspiel 2004).

The ACTIBIO recordings gave the opportunity to have real data to be used to evaluate the system authentication performances. Relevant data for the SensingSeat system were collected in a fixed seat office scenario, giving to the users the opportunity to act according to a specified protocol. The actions have been chosen in order to simulate in the best way a real office scenario. The main activities are answer to phone, typing, using the mouse, writing with a pencil, taking a glass. The list of the actions for the events triggering are shown below (Table 5.2).

As previously explained, the data have been analysed with some algorithms in the way to test and chose the that one with best performance. The classifier VDC, based on Euclidean vector distance, was trained on 80% of the available examples for each action and subject, while the remaining 20% was used as the test set. The results in term of FAR and FRR for each action and for each subject are shown in the figures below. The data were analyzed in order to classify each subject, with respect to the all the others, performing each action (Figs. 5.13 and 5.14).

The results show a mean FAR=0.9% +/-3.1% and a mean FRR equal to 0.1% +/-0.4%. Even if the results are encouraging, more tests must be conducted since the number of repetitions per action and subject is currently too small to assess the system reliability. The EER is calculated for each specific activities; in the following

Table 5.2 The actions used for the event-related authentication analysis

Action ID	Action description
0	Phone conversation
1	Phone conversation (light)
2	Phone reached the ear
3	Phone left from ear
4	Interacting with mouse
5	Interacting with mouse (light)
6	Write typing
7	Write typing (light)
8	Writing with pencil
9	Writing with pencil (light)
10	Talking to the microphone panel
11	Talking the microphone panel (light)
12	Pressing buttons in the office panel
13	Pressing buttons in the office panel (light)
14	Drinking from glass
15	Drinking from glass (light)
16	Filling glass with water
17	Yawning
18	Raising hands
19	User is seated
20	Watching video
21	No activity

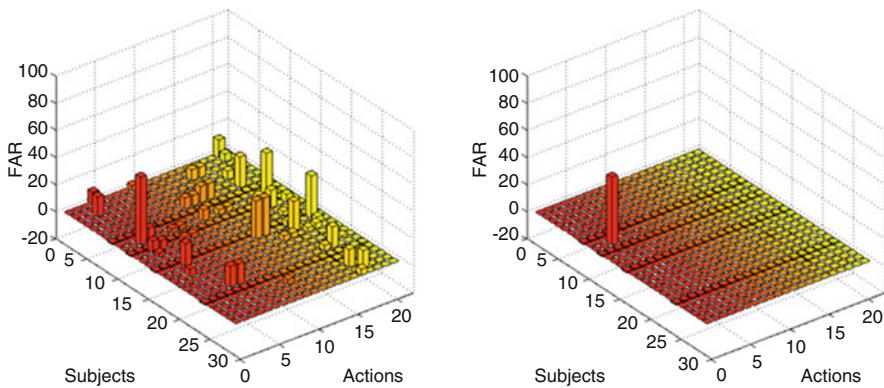


Fig. 5.13 SensingSeat authentication error: FAR and FRR (24 subjects, 21 actions, 6 repetitions per subject per action)

figures, for simplicity, the “Phone reached the ear” and “Phone conversation” actions are shown, considering for instance the subject 13. The EER is calculated for the considered subject performing the specific action with respect to all the other subjects. This parameter permits to see how the system is able to recognize a subject during a specific event, and to see how it is able to distinguish the considered subject respect to all the others (Fig. 5.15).

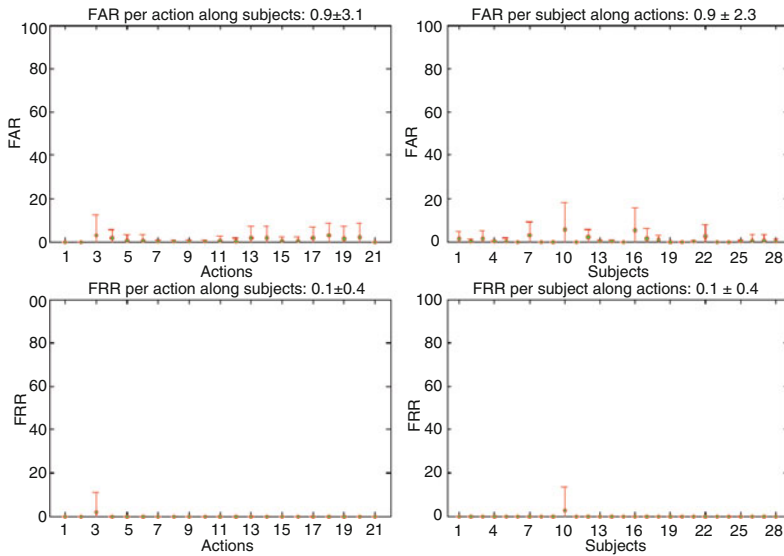


Fig. 5.14 SensingSeat authentication error: mean and standard deviation of FAR and FRR along subjects (*left*) and actions (*right*); 24 subjects, 21 actions, 6 repetitions per subject per action

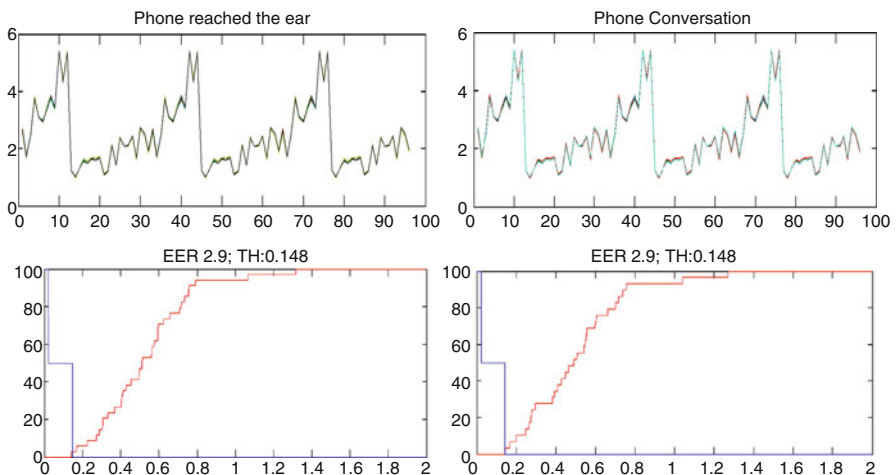
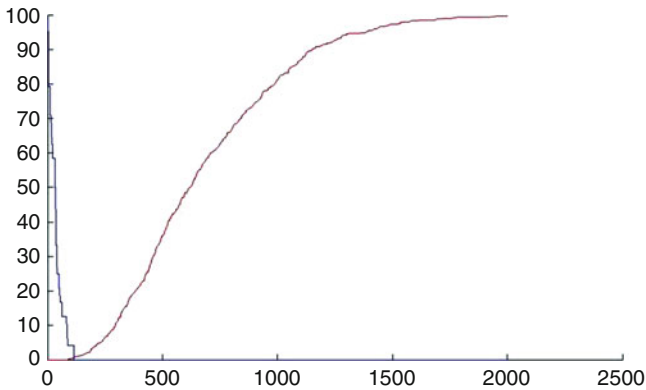


Fig. 5.15 Subject ID 13: comparison of two actions: “Phone reached the ear” (*left*) and “Phone conversation” (*right*); the features are shown at the *top*; the FRR and FAR vs. threshold curve is shown at the *bottom*

Considering the global performance of the system, the best useful parameter is the EER calculated for each action considering all the subject. In the following table the results are reported (Table 5.3).

Table 5.3 EER calculated for every actions considering all the subjects

Action ID	Action description	EER per action
0	Phone conversation	1.268
1	Phone conversation (light)	1.087
2	Phone reached the ear	2.536
3	Phone left from ear	5.435
4	Interacting with mouse	0.867
5	Interacting with mouse (light)	0.945
6	Write typing	1.087
7	Write typing (light)	1.087
8	Writing with pencil	2.355
9	Writing with pencil (light)	0.925
10	Talking to the microphone panel	4.167
11	Talking the microphone panel (light)	4.167
12	Pressing buttons in the office panel	1.345
13	Pressing buttons in the office panel (light)	1.449
14	Drinking from glass	4.167
15	Drinking from glass (light)	4.167
16	Filling glass with water	2.213
17	Yawning	3.456
18	Raising hands	8.333
19	User is seated	4.456
20	Watching video	6.703
21	No activity	3.442

**Fig. 5.16** EER calculated for “Interacting with the mouse” considering all the subjects. The value of EER is 0.867

With respect to the previous summarizing table, it is possible to show the comparison between the actions with the best and the worst score, respectively “Interacting with the mouse” and “Raising hand” (Figs. 5.16 and 5.17).

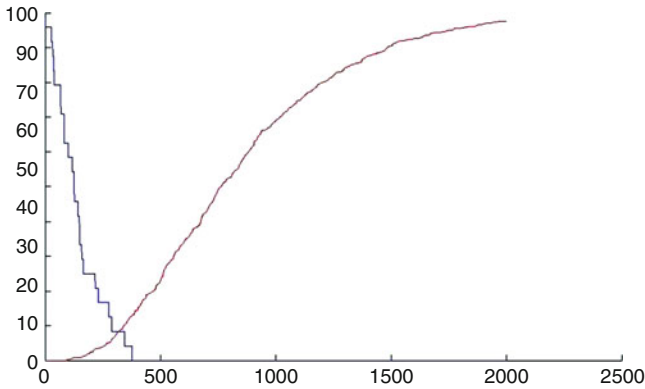


Fig. 5.17 EER calculated for “Raising hand” considering all the subjects. The value of EER is 8.333

5.4.2.2 Conclusions

In this section the development of a novel sensing seat system based on an unobtrusive piezoresistive sensor array is described. The main result is a positive assessment of the use of the reported sensing seat in the authentication task, showing the robustness of the system in terms of biometric rates. Another relevant result is the assessment of the strain sensor technology and of the classification modules based on personal and event-related classifiers. The proposed system is still under development even if the actual prototype was successfully tested within unimodal and multimodal environments. The main advantage in respect of the previous Sensing Seat prototype is represented by the absence of the cooperation of the human subject during the monitoring stage. The open issues include the performance study in extreme environmental conditions (e.g. very low and very high environmental temperature scenarios). Moreover, the strain sensor stability over time as well as its chemical properties must be investigated thoroughly in order to study the sensor degeneration over time (i.e. sensor aging). Additionally, in order to make the system really unobtrusive, the objects inside the clothes and the pockets (e.g. keys, wallet) should be treated as a point of disturbance to increase the final user convenience. All the above mentioned topics will be taken into account in future developments.

5.5 Concluding Remarks

Biometrics measure physical or behavioral characteristics of an individual in order to recognize or authenticate their identity. Usually fingerprints, hand or palm geometry, retina, iris, or facial characteristics are used as physical biometric variables. Signature, voice (which also has a physical component), keystroke pattern and gait are included in behavioral characteristics.

Although some technologies have gained more acceptance than others, it is beyond doubt that the field of access control and biometrics as a whole shows great potential for use in end user segments, such as airports, stadiums, defence installations but also the industry and corporate workplaces where security and privacy are required.

In this chapter, two emerging biometric technologies, namely Gait and Anthropometric profile, have been presented that exploit the human static and dynamic body characteristics for human recognition. Even if these technologies are mature, their high authentication accuracy has been demonstrated and their deployment in existing or new biometric security solutions has been indicated in order to: (i) improve the reliability and accuracy of the multimodal biometric frameworks, (ii) provide new means of unobtrusive subject authentication based on activity-related signals and (iii) to ignite further research on emerging and second generation of biometrics that exploit high recognition performance and take into account user privacy and convenience.

References

- Abate, A.F., M. Nappi, D. Riccio, and G. Sabatino. 2007. 2D and 3D face recognition: Survey. *Pattern Recognition Letters* 28(14): 1885–1906.
- Bodor, R., A. Drenner, D. Fehr, O. Masoud, and N. Papanikolopoulos. 2009. View-independent human motion classification using image-based reconstruction. *Image and Vision Computing* 27(8): 1194–1206.
- Bouchrika, I., and M. Nixon. 2007. Model-based feature extraction for gait analysis and recognition. *Computer vision/computer graphics collaboration techniques*, 150–160.
- Bouchrika, I., and M. Nixon. 2008. Gait recognition by dynamic cues. In *19th IEEE International Conference on Pattern Recognition, 2008*, Tampa, FL, USA.
- Bouchrika, I., M. Goffredo, J. Carter, and M. Nixon. 2009. Covariate analysis for view-point independent gait recognition. In *The 3rd IAPR/IEEE International Conference on Biometrics*, Italy.
- Boulgouris, N.V., Chi, Z.X., 2007 “Gait recognition using radon transform and linear discriminant analysis,” *IEEE Transactions on Image Processing* 16(3): 731–740, March 2007.
- Boulgouris, N.V., K.N. Plataniotis, and D. Hatzinakos. 2004. Gait recognition using dynamic time warping. In *IEEE 6th Workshop on Multimedia Signal Processing*, 263–266, September 29–October 1, 2004.
- Boulgouris, N.V., D. Hatzinakos, and K.N. Plataniotis. 2005. Gait recognition: A challenging signal processing technology for biometric identification. *IEEE Signal Processing Magazine* 22(6): 78–90.
- Bowyer, K.W., K. Hollingsworth, and P.J. Flynn. 2008. Image understanding for iris biometrics: A survey. *Computer Vision and Image Understanding* 110(2): 281–307.
- Chen, C., J. Liang, H. Zhao, H. Hu, and J. Tian. 2009. Frame difference energy image for gait recognition with incomplete silhouettes. *Pattern Recognition Letters* 30(11): 977–984.
- Cucchiara, R., C. Grana, M. Piccardi, A. Prati, and S. Sirotti. 2001. Improving shadow suppression in moving object detection with HSV color information. In *2001 IEEE Intelligent Transportation Systems Proceedings*, 334–339.
- Daras, P., D. Zarpalas, D. Tzovaras, and M.G. Strintzis. 2006. Efficient 3-D model search and retrieval using generalized 3-D radon transforms. *IEEE Transactions on Multimedia* 8(1): 101–114.
- Federspiel L. Sensor mat for a vehicle seat. I.E.E. International Electronics & Engineering S.a.r.l. Patent, US6794590, Sept. 2004.

- Ferro, M., G. Pioggia, A. Tognetti, N. Carbonaro, and D. De Rossi. 2009. A sensing seat for human authentication. *Transactions on Information Forensics and Security* 4(3): 451–459.
- Ford Global Technologies Inc. Vehicle air bag deployment dependent on sensing seat and pedal positions. Patent, priorities: [US09681903 Jun. 22, 2001], UKC Headings: G4N Int C17 B60R 21/01, B60R 21/16, GB2377536 (GB0212617.5), May 2002.
- Gloor, P.A. 1980. Bertillon's method and anthropological research; A new use for old anthropometric files. *Journal of the Forensic Science Society* 20(2): 99–101. ISSN 0015–7368.
- Goffredo, M., J.N. Carter, and M.S. Nixon. 2008. Front-view gait recognition. In *IEEE Second International Conference on Biometrics: Theory, Applications and Systems, BTAS*.
- Hilliard G.G. Seat cushion. Patent, GB0228513.8, Dec. 2002.
- Ioannidis, D., D. Tzovaras, I.G. Damousis, S. Argyropoulos, and K. Moustakas. 2007. Gait recognition using compact feature extraction transforms and depth information. *IEEE Transaction Information Forensics and Security* 2: 623–630.
- Jain, A.K., A. Ross, and S. Prabhakar. 2004. An introduction to biometric recognition. *IEEE Transactions on Circuits and Systems for Video Technology* 14(1): 4–20.
- Jean, F., Alexandra Branzan Albu, and Robert Bergevin. 2009. Towards view-invariant gait modeling: Computing view-normalized body part trajectories. *Pattern Recognition* 42(11): 2936–2949.
- Lorussi, F., W. Rocchia, E.P. Scilingo, A. Tognetti, and D. De Rossi. 2004. Wearable redundant fabric-based sensors arrays for reconstruction of Body segment posture. *IEEE Sensors Journal* 4(6): 807–818.
- Lorussi, F., E.P. Scilingo, M. Tesconi, A. Tognetti, and D. De Rossi. 2005. Strain sensing fabric for hand posture and gesture monitoring. *IEEE Transactions on Information Technology in Biomedicine* 9(3): 372–381.
- Mademlis, A., A. Axenopoulos, P. Daras, D. Tzovaras, and M.G. Strintzis. 2006. 3D content-based search based on 3D Krawtchouk moments. In *3DPVT 2006*, University of North Carolina, Chapel Hill, NC, USA, June 2006.
- Moustakas, K., D. Tzovaras, and M.G. Strintzis. 2007. SQ-Map: Efficient layered collision detection and haptic rendering. *IEEE Transactions on Visualization and Computer Graphics* 13(1): 80–93.
- Salembier, P., and F. Marqués. 1999. Region-based representations of image and video: Segmentation tools for multimedia services. *IEEE Transactions on Circuits and Systems for Video Technology* 9(8): 1147–1169.
- Sarkar, S., P.J. Phillips, Z. Liu, I.R. Vega, P. Grother, and K.W. Bowyer. 2005. The human ID gait challenge problem: Data sets, performance, and analysis. *IEEE Transaction Pattern Analysis and Machine Intelligence* 27(2): 162–177.
- Scilingo, E.P., F. Lorussi, A. Mazzoldi, and D. De Rossi. 2003. Sensing fabrics for wearable kinaesthetic-like systems. *IEEE Sensors Journal* 3(4): 460–467.
- Tan, H.Z., L.A. Slivovsky, and A. Pentland. 2001. A sensing chair using pressure distribution sensors. *IEEE/ASME Transactions on Mechatronics* 6(3): 261–268.
- The Johnson Controls Company. <http://www.johnsoncontrols.com/>. Accessed on 17 Mar 2008.
- The Softswitch Company. <http://www.softswitch.co.uk/>. Accessed on 17 Mar 2008.
- The Tekscan Company. <http://www.tekscan.com>. Accessed on 17 Mar 2008.
- The Wacker Company. The grades and properties of Elastosil LR liquid silicon rubber. http://www.wacker.com/internet/webcache/de_DE/_Downloads/EL_LR_Eigensch_en.pdf. Accessed on 17 Mar 2008.
- Zhang, R., C. Vogler, and D. Metaxas. 2007. Human gait recognition at sagittal plane. *Image and Vision Computing* 25: 321–330.